The Dynamic Behavior and Compliance of a Stream of Cavitating Bubbles

C. BRENNEN

Senior Research Fellow in Engineering Science, California Institute of Technology, Pasadena, Calif.

The role played by turbopump cavitation in the POGO instability of liquid rockets motivates the present study on the dynamic response of streams of cavitating bubbles to imposed pressure fluctuations. Both quasistatic and more general linearized dynamic analyses are made of the perturbations to a cavitating flow through a region of reduced pressure in which the bubbles first grow and then collapse. The results when coupled with typical bubble number density distribution functions yield compliances which compare favorably with the existing measurements. Since the fluids involved are frequently cryogenic, a careful examination was made of the thermal effects both on the mean flow and on the perturbations. As a result the discrepancy between theory and experiment for particular engines could be qualitatively ascribed to reductions in the compliance caused either by these thermal effects or by relatively high reduced frequencies.

1 Introduction

THE importance of the POGO instability in the operation of liquid propellant rockets [1, 2][1] and the role played by the fuel and oxidizer turbopumps in that instability has focused renewed attention on theoretical means for predicting the response of cavitating inducers to oscillatory pressure and mass flows. The pump transfer function relating the inflow and outflow pressures and mass flows is, in general, a matrix with four complex components yielding eight separate characteristics. Of these, the cavitation compliance [2, 3], C_B, defined by

$$C_B = -\rho_L \partial V_C / \partial P_\infty \tag{1}$$

where ρ_L is the liquid density, V_C is the total volume of the vapor or gas cavities, and P_∞ is the suction pressure, appears to be of particular interest to the dynamicists [2]. This generally complex quantity represents the dependence of the difference between the inlet and outlet flows (or cavity volume growth) on the fluctuating suction pressure which causes it. It will, in general, be a function of the frequency, Ω, of the perturbations.

Cavitation appears in a number of forms in a typical axial inducer [3, 4, 5]. Nuclei, present in the inflow, may grow explosively (cavitate) as they are convected through the low pressure region on the suction side of the inducer blades, finally collapsing when they are convected to regions of higher pressure. Though it is not possible to establish a precise line between the various forms of cavitation, this will be termed bubble cavitation. As the cavitation number, σ, is reduced a single vaporous wake, or full developed cavity, will form on the suction side of the blade. This is termed blade cavitation and, in turbopumps,

[1]Numbers in brackets designate Ref erences at end of paper.

Contributed by the Fluids Engineering Division and presented at the Applied Mechanics and Fluids Engineering Conference, Atlanta, Ga., June 20–22, 1973, of THE AMERICAN SOCIETY OF MECHANICAL ENGINEERS. Manuscript received at ASME Headquarters, April 4, 1973. Paper No. 73-FE-34.

Nomenclature

A = local constant
A_i = inducer inlet area
C_B = turbopump compliance
C_P = pressure coefficient, $(P - P_\infty)/{}^1/_2\rho_L U^2$
C_{P0} = mean flow pressure coefficient
C_{PM} = minimum pressure coefficient
C_{P1} = pressure coefficient oscillation amplitude
c_{PL} = specific heat of liquid
D = thermal diffusivity of liquid
f = nondimensional frequency
F_1, F_2, F_3 = thermodynamic functions
G = thermal effect function
j = imaginary unit
K_B = dimensionless total compliance, $C_B U^2/2LA_i$
K_C = total unit compliance
K_L = local unit compliance
k_L = thermal conductivity of liquid
L = typical reduced pressure length
$\mathcal{L}$ = latent heat of evaporation
$\dot{M}$ = mass rate of vapor production
N^* = bubble number density distribution function

(Continued on next page)

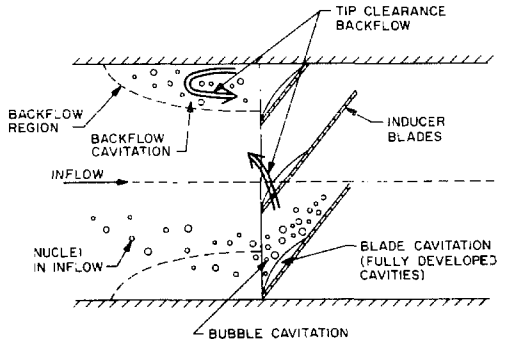

Fig. 1 Schematic illustrating forms of cavitation for an axial inducer

commonly occurs alongside bubble cavitation. In addition, it is useful to identify a third type associated with the tip clearance flows which in the highly loaded inducers of rocket engine turbopumps often produce backflows. Then the term backflow cavitation refers to the cavitation in the vortices shed by the blade tips and any other bubbles convected by this reversed stream. These characteristic cavitation forms are illustrated in Fig. 1.

Blade cavitation in a turbopump and the compliance it yields have been explored by a number of authors [3, 6, 7]. Brennen and Acosta [6, 7] obtained theoretical results for the quasistatic or low frequency compliance due to blade cavitation in a number of existing turbopumps by employing a finite cavity cascade theory. (The corresponding general dynamic problem has been addressed by Kim [8] with the objective of finding the frequency dependence of the blade compliance.) The real and positive compliance values obtained were substantially smaller than the existing experimental measurements [6, 7]. However, serious doubts are expressed concerning the validity of these indirect experimental observations and a satisfactory comparison must await more direct measurements of pump transfer functions. Nevertheless it is clearly of importance to explore other sources of compliance and therefore the contributions from other forms of turbopump cavitation. Since both bubble and backflow cavitation involve streams of bubbles it is important to know some of the general features of the compliance of a stream of cavitation bubbles. It is worth noting at this point that helium bubbles are sometimes introduced into the feed lines in order to provide the total system with additional compliance. The nuclei gas content referred to later would thus include this situation.

Therefore, the purpose of this paper is to investigate both the quasistatic and more general dynamic response of a stream of cavitating bubbles to fluctuations in the basic suction pressure. This will form a theoretical base from which to explore the compliance of bubble and backflow cavitation and empirical observations such as those of Ghahremani [10]. No attempt has, as yet, been made to reproduce the conditions in the main stream or backflow of a particular turbopump. Instead a general, simple mean pressure distribution for the stream has been employed with the objective of establishing general trends without excessive computation. It should be pointed out that values for the compliance of a stream with uniform mean pressure are available in existing works [11] though it is not termed "compliance." For example, the "frequency response function" of Hsu and Watts [11] is proportional to the compliance as will become evident below. However, most of the following calculations differ in that they are concerned with a cavitating stream in which the mean pressure is far from uniform.

Most of the experimental data mentioned above have been obtained from tests in which water has been used as the working fluid, rather than the actual liquids (commonly cryogenic) for which turbopumps were designed. But the thermodynamic properties of these liquids at the operating temperature may be radically different from those of water. For this reason, the thermal effects on both the mean flow and on the perturbations, which depend in turn on the respective time-scales of the two motions, are considered and evaluated. Thermal effects on cavitating (mean) flows and the difference between cavitation and boiling have been extensively examined in the past, particularly by Plesset [12, 13, 14]. It was, however, considered appropriate to include in Section 4 a variation on Plesset's analysis in order to present an explicit formula which may permit a determination of whether a particular flow of a given liquid will cavitate or boil. Additional thermal effects on the fluctuations are evaluated in Section 8.

2 Bubble Motion

A number of simplifying basic assumptions concerning the bubble motion are necessary in order to create a tolerably soluble problem. It is assumed (I) that the bubbles have their origin in nuclei present in the inflow, (II) that relative motion between the bubbles and the fluid immediately surrounding them can be neglected, and (III) that the bubbles are sufficiently far apart for each to be unaffected by the growth or collapse of neighboring bubbles. Then the bubble growth will be governed by the Rayleigh-Plesset equation [12]

Nomenclature

$N = N^*L^4$
P = pressure
P_∞ = remote pressure in liquid
P_B = total pressure in bubble
P_V = vapor pressure
P_G = partial pressure of gas
$\dot{Q}_T$ = heat flux into bubble
$\dot{Q}_G$ = rate of heat absorbed by gas
$\dot{Q}_{V0}$ = rate of heat absorbed by vapor
r = dimensionless bubble radius, R/L
r_N = dimensionless nuclei radius, R_N/L
r_0 = mean flow size history
r^* = perturbed flow size history
r_1 = radius oscillation amplitude
r_N^* = perturbed nuclei size
R = bubble radius
R_N = nuclei radius
Re = Reynolds number, UL/ν
S = surface tension
t = dimensionless time, t_1U/L
t_1 = time
T = temperature
T_∞ = remote temperature in liquid
T_B = temperature in bubble
T_T = triple point temperature
T_C = critical point temperature
U = velocity of stream
V_C = total cavity volume
We = Weber number, $\rho_L U^2 L/S$
Y = radius from bubble center
α = thermodynamic function, $\mathcal{L}\rho_V/P_V$
$\beta = 2P_V/\rho_L U^2$
γ_G = ratio of specific heats of gas
γ_V = ratio of specific heats of vapor
ϵ = local constant
θ = temperature deviation $(T - T_\infty)/T_\infty$
$\theta_B = (T_B - T_\infty)/T_\infty$
θ_{B1} = amplitude of θ_B oscillations
ν = kinematic viscosity of liquid
ρ_L = liquid density
ρ_V = vapor density
σ = cavitation number, $(P_\infty - P_V(T_\infty))/\frac{1}{2}\rho_L U^2$
Σ = thermal effect function
$\omega = 2\pi f$
ω_n = natural bubble frequency
Ω = dimensional frequency, $U\omega/L$

$$R\frac{d^2R}{dt_1^2} + \frac{3}{2}\left(\frac{dR}{dt_1}\right)^2 = \frac{P_B(T_B) - P(t_1)}{\rho_L} - \frac{2S}{\rho_L R} - \frac{4\nu}{R}\frac{dR}{dt_1} \quad (2)$$

where t_1 is time, R the radius of the bubble, ρ_L the liquid density, S the surface tension, and ν the kinematic viscosity. Given the pressure history along the trajectory of the bubble in the latter's absence, $P(t_1)$, the solution of this equation yields the size/time history, $R(t_1)$. Only the internal bubble pressure $P_B(T_B)$ requires further comment. It is assumed to consist of the vapor pressure $P_V(T_B)$ of the liquid at the internal bubble temperature T_B and a partial pressure, $P_G(T_B)$, due to a mass of gas in the bubble; this mass is assumed to remain unchanged throughout the motion since the typical time for gas diffusion in the liquid is usually large compared with the growth time. Then assuming the nucleus (of size $R = R_N$) from which the bubble grows is in equilibrium at a constant pressure, P_∞, upstream of the low pressure region it follows from (2) that

$$(P_B)_{R=R_N} = P_\infty + \frac{2S}{R_N} \quad (3)$$

In this region the bubble temperature will be identical to the remote stream temperature, T_∞, so that the vapor pressure in the nuclei will be $P_V(T_\infty)$; it follows that the partial pressure of gas, P_G, is

$$(P_G)_{R=R_N} = P_\infty + \frac{2S}{R_N} - P_V(T_\infty) \quad (4)$$

Obtaining the partial pressure of the gas at any radius and temperature from the perfect gas law, the pressure term in equation (2) can be replaced by

$$P_B(T_B) - P(t_1) = -(P - P_\infty) - (P_\infty - P_V(T_\infty)) + (P_V(T_B) - P_V(T_\infty)) + \{P_\infty + 2S/R_N - P_V(T_\infty)\}(R_N/R)^3(T_B/T_\infty) \quad (5)$$

where the last term represents the partial pressure of the gas. It is convenient for future purposes to nondimensionalize the equations at this stage and to assume that the bubble temperature deviation $\theta_B = (T_B - T_\infty)/T_\infty$ is sufficiently small to expand in Taylor series

$$P_V(T_B) - P_V(T_\infty) \simeq -\theta_B \left\{ T\frac{\partial P_V}{\partial T} \right\}_{T=T_\infty} = -\mathcal{L}\rho_V\theta_B \quad (6)$$

where the latent heat of vaporization, $\mathcal{L}$, and saturated vapor density, ρ_V, may be evaluated at $T = T_\infty$. The last relation follows from the Clausius-Clapeyron equation. The resulting dimensionless momentum equation for bubble growth becomes

$$2r\frac{d^2r}{dt^2} + 3\left(\frac{dr}{dt}\right)^2 + C_P(t) + \sigma - \alpha\beta\theta_B + \frac{8}{r\,\mathrm{Re}}\frac{dr}{dt} + \frac{4}{r\,\mathrm{We}} = (\theta_B + 1)\left(\frac{r_N}{r}\right)^3\left\{\sigma + \frac{4}{\mathrm{We}\,r_N}\right\} \quad (7)$$

where, if U and L are typical velocity and length, $r = R/L$, $t = t_1U/L$, $C_P = (P - P_\infty)/\frac{1}{2}\rho_LU^2$, the cavitation number, $\sigma = (P_\infty - P_V(T_\infty))/\frac{1}{2}\rho_LU^2$, the Reynolds number, $\mathrm{Re} = UL/\nu$, the Weber number, $\mathrm{We} = \rho_LU^2L/S$, α is the thermodynamic property, $\mathcal{L}\rho_V/P_V$, and $\beta = P_V/\frac{1}{2}\rho_LU^2$.

The basic difference between cavitation and boiling has been extensively examined in the past, particularly by Plesset [12, 13, 14]. Cavitation generally occurs at low liquid temperatures where the bubble growth is impeded only by liquid inertia and not by thermal diffusion. The temperature of the bubble content remains virtually unchanged. Thus for a given $C_P(t)$, cavitation bubble motion can be described completely by equation (7) with θ_B set equal to zero. At higher temperatures however, bubble growth may be severely restricted by the rate at which heat can diffuse toward the interface in order to vaporize the liquid. In such a situation the process is termed boiling in order to distinguish it from cavitation. Indeed in many liquid flows there is a transitional temperature range below which bubble growth will take the form of cavitation and above which boiling will occur. In order to examine these thermal effects the thermodynamic equations for the growth of a vapor/gas bubble are outlined in the next section.

3 Thermodynamic Equations of Bubble Motion

The inclusion of thermal effects requires an energy equation to supplement (7) and allow simultaneous solution for both $r(t)$ and $\theta_B(t)$. This, in turn, requires the solution of the equation for heat diffusion in the liquid [14]

$$\frac{\partial T}{\partial t_1} + \frac{R^2}{Y^2}\frac{dR}{dt_1}\frac{\partial T}{\partial Y} = D\left\{\frac{\partial^2 T}{\partial Y^2} + \frac{2}{Y}\frac{\partial T}{\partial Y}\right\} \quad (8)$$

where D is the thermal diffusivity of the liquid, T is the temperature at a point in the liquid of radius, Y, and $(T)_{Y=R} = T_B$. The heat flux into the bubble, $\dot{Q}_T$, is then

$$\dot{Q}_T = 4\pi R^2 k_L\left(\frac{\partial T}{\partial Y}\right)_{Y=R} \quad (9)$$

where k_L is thermal conductivity of the liquid. But if γ_G is the ratio of specific heats of the gas in the bubble, the heat, $\dot{Q}_G$, absorbed by this mass of gas is

$$\dot{Q}_G = \frac{4}{3}\pi R_N^3\left\{P_\infty - P_V(T_\infty) + \frac{2S}{R_N}\right\}\left\{\frac{1}{(\gamma_G - 1)}\frac{dT_B}{dt_1} + \frac{3T_B}{R}\frac{dR}{dt_1}\right\}/T_\infty \quad (10)$$

and the rate at which heat is absorbed by the mass of vapor in the bubble, $\dot{Q}_{V0}$, is

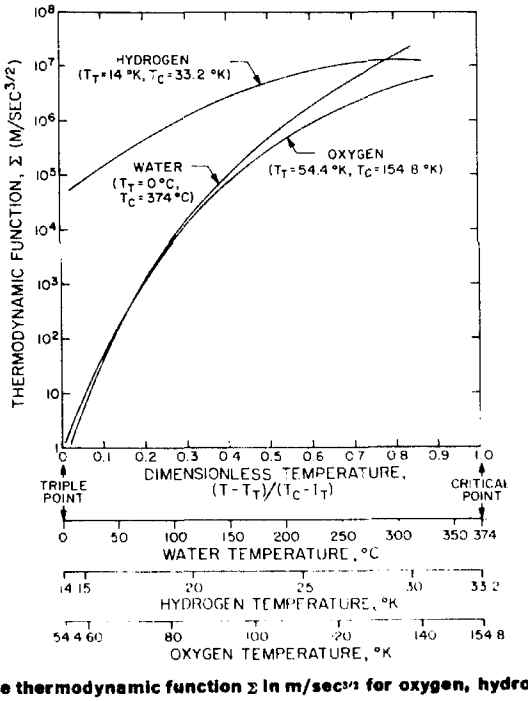

Fig. 2 The thermodynamic function Σ in m/sec$^{3/2}$ for oxygen, hydrogen and water

$$\dot{Q}_{V0} = \frac{P_V(T_B)}{T_B}\ \frac{4}{3}\pi R^3 \left\{ \frac{1}{(\gamma_V - 1)}\frac{dT_B}{dt_1} + \frac{3T_B}{R}\frac{dR}{dt_1} \right\} - \frac{P_V(T_B)M}{\rho_V(T_B)} \qquad (11)$$

where $\dot{M}$ is the mass rate of production of vapor at the interface, γ_V is the ratio of specific heats of the vapor, and $\rho_V(T_B)$ the saturated vapor density. Now the total mass of vapor in the bubble is $4\pi R^3\rho_V(T_B)/3$ or

$$\dot{M} = \frac{4\pi R^3\rho_V(T_B)}{3}\left\{ \frac{3}{R}\frac{dR}{dt_1} + \left(\frac{1}{\rho_V}\frac{d\rho_V}{dT}\right)_{T=T_B}\frac{dT_B}{dt_1} \right\}. \qquad (12)$$

But since the heat flow remaining to evaporate the liquid is $(\dot{Q}_T - \dot{Q}_G - \dot{Q}_{V0})$ the mass rate of production of vapor must also be

$$\dot{M} = (\dot{Q}_T - \dot{Q}_G - \dot{Q}_{V0})/\mathcal{L}(T_B). \qquad (13)$$

Eliminating $\dot{M}$ from the above and using the Clausius-Clapeyron relation yields the energy equation

$$\frac{dR}{dt_1}\left\{ \mathcal{L}(T_B)\rho_V(T_B) + \frac{R_N^3}{R^3}\frac{T_B}{T_\infty}\left(P_\infty - P_V(T_\infty) + \frac{2S}{R_N}\right)\right\} + \frac{R}{3T_B}\frac{dT_B}{dt_1}\left[P_V(T_B)\left\{ \frac{\mathcal{L}(T_B)\rho_V(T_B)}{P_V(T_B)} - 1\right\}^2 + \frac{P_V(T_B)}{(\gamma_V - 1)} + \frac{R_N^3}{R^3}\frac{T_B}{T_\infty}\frac{\left(P_\infty - P_V(T_\infty) + \frac{2S}{R_N}\right)}{(\gamma_G - 1)}\right] = k_L\left(\frac{\partial T}{\partial Y}\right)_{Y=R}. \qquad (14)$$

The nondimensional, small perturbation form of this equation which is to be used later is obtained by assuming that $\theta_B << 1$. To the first order the variation of $\mathcal{L}$, ρ_V, and P_V with θ_B can be neglected since the quantities occur in the coefficients of dr/dt and $d\theta_B/dt$. Then

$$\frac{dr}{dt}\left[\alpha\beta + \left(\frac{r_N}{r}\right)^3(\sigma + 4/\mathrm{We}\, r_N)\right] + \frac{r}{3}\frac{d\theta_B}{dt}\left[\beta((\alpha - 1)^2 + (\gamma_V - 1)^{-1}) + \left(\frac{r_N}{r}\right)^3(\gamma_G - 1)^{-1}(\sigma + 4/\mathrm{We}\, r_N)\right] = \left\{\frac{2k_LT_\infty}{\rho_LU^3L}\right\}\left(\frac{\partial\theta}{\partial y}\right)_{y=r}. \qquad (15)$$

The nondimensional form of (8) is

$$\frac{\partial\theta}{\partial t} + \frac{r^2}{y^2}\frac{dr}{dt}\frac{\partial\theta}{\partial y} = \left\{\frac{D}{UL}\right\}\left(\frac{\partial^2\theta}{dy^2} + \frac{2}{y}\frac{\partial\theta}{\partial y}\right). \qquad (16)$$

4 Cavitation and Boiling in Water and Cryogenic Liquids

To investigate the dynamics of a cavitating (or boiling) flow both a mean flow and an oscillatory perturbation to that mean flow will be established. Both will have their own, possibly radically different thermal effects. But since a complete solution of equations (7), (15), and (16) is excessively complex for present purposes, a phenomenonolgically selective course of action has been taken. The primary objective of this paper has been to study *cavitating* mean flows, their compliance and the thermal effects on that compliance. The bubble growth in *boiling* mean flows is much less rapid than in the cavitating case; thus as a first approximation, the latter can be regarded in the light of results for a *uniform* mean flow.

It is clearly of importance to be able to establish *a priori* whether the mean flow is one which will cavitate or boil. Strangely, though some particular examples have been delineated in the literature [12, 13, 14] there exists no explicit formula from which an estimate can be made of the transitional temperature in a particular liquid and for a given flow situation. Since such a formula is relatively easily obtained by employing a variation on the analysis of Plesset [14] it was considered appropriate to include the following short digression in this paper and to suggest such an explicit formula.

Consider the condition required for boiling. If the inertial terms in equation (7) can be neglected and the influence of the surface tension and gaseous terms are also, for the present purpose, neglected then

$$\theta_B \approx \frac{1}{\alpha\beta}\ C_P(t). \qquad (17)$$

If the diffusion layer surrounding the bubble is small then an approximate local solution to (16) is

$$\theta \cong A\exp\left\{ \frac{D}{UL}\epsilon^2 t - \epsilon(y - r)\right\} \qquad (18)$$

where A and ϵ are local constants which may be eliminated to yield

$$\left(\frac{\partial\theta}{\partial y}\right)_{y=r} = -\left[\left\{\frac{UL}{D}\right\}\theta_B\frac{d\theta_B}{dt}\right]^{\frac{1}{2}} \qquad (19)$$

A study of the thermodynamic properties of most liquids reveals that at the higher, boiling temperatures the prominent terms in the energy equation (15) are

$$\alpha\beta\frac{dr}{dt} \approx +\left\{\frac{2k_LT_\infty}{\rho_LU^3L}\right\}\left(\frac{\partial\theta}{\partial y}\right)_{y=r}. \qquad (20)$$

Substituting θ_B from (19) and (17) it follows that

$$\frac{dr}{dt} \approx -\frac{1}{\alpha^2\beta}\left\{\frac{D^{\frac{1}{2}}T_\infty c_{PL}\rho_L}{P_VL^{\frac{1}{2}}U^{\frac{1}{2}}}\right\}\left(C_P\frac{dC_P}{dt}\right)^{\frac{1}{2}}. \qquad (21)$$

But, returning to the original premise the condition for boiling rather than cavitation is that the inertial terms in (7) be small compared with say C_P; thus one condition is

$$\left(\frac{dr}{dt}\right)^2 << C_P.$$

Comparing this with (21) yields a condition on dC_P/dt. But dC_P/dt is of the same order as σ so it follows that boiling will occur when

$$\left(\frac{U^3\sigma}{L}\right)^{\frac{1}{2}} << \left[\frac{2\mathcal{L}^2\rho_V^2}{D^{\frac{1}{2}}c_{PL}T_\infty\rho_L^2}\right] \equiv \Sigma(T). \qquad (22)$$

This defines a transitional temperature for a particular flow process. When the flow property, $(U^3\sigma/L)^{1/2}$, is much smaller than the thermodynamic property of the liquid/vapor, $\Sigma(T)$, boiling will occur; in reverse circumstances, cavitation will take place.

Values of $\Sigma(T)$ for water, normal hydrogen, and oxygen are plotted against a dimensionless temperature, $(T - T_T)/(T_C - T_T)$ (where T_T is the triple point, T_C the critical point temperature) in Fig. 2. Given the value of $(U^3\sigma/L)^{1/2}$ for a particular flow, the transitional temperature is then easily obtained from this figure. For example with typical turbopump values of $U \approx 100$ m/sec, $L \approx 0.5$m, and $\sigma \approx 0.1$ it follows that $(U^3\sigma/L)^{1/2} \approx 400$ m/sec$^{3/2}$. Under these conditions liquid oxygen would cavitate rather than boil below about 70 deg K, liquid hydrogen would virtually always boil and water would cavitate below about 60 deg C.

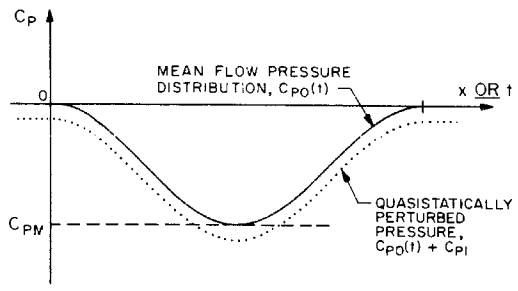

Fig. 3 Remote pressure history

Unfortunately there does not appear to be a great awareness of these distinctions in the literature. Thus despite the fact that liquid hydrogen will boil rather than cavitate in virtually all practical flow situations, experimental investigations with LH_2 such as those of Stinson and Strickland [15] and Hord, Anderson, and Hall [16] still regard the bubble growth in "cavitating" terms.

5 Cavitation Bubble Motion—The Mean Flow

In order to study the response of a cavitating flow to imposed perturbations, a basic or mean flow must first be established. Toward this end numerical solutions for the cavitation form of equation (7) (i.e., with $\theta_B = 0$) were obtained by means of a second order Runge Kutta procedure utilizing the initial conditions

$$r(0) = r_N, \left(\frac{dr}{dt}\right)_{t=0} = 0. \tag{23}$$

In order to reduce the total number of variables, typical values for We and Re were chosen as 10^8 and 10^7, respectively, and these parameters whose effect is relatively small remain unchanged throughout the data presented. In addition, a simple but typical mean pressure history of the form, $C_P(t) = C_{P0}(t)$ was assumed where, as indicated in Fig. 3,

$$\begin{aligned} C_{P0}(t) &= 0 \qquad\qquad , t \leq 0 \text{ and } t > 1 \\ C_{P0}(t) &= C_{PM} \sin^2 \pi t,\ C_{PM} \text{ negative},\ 0 < t < 1. \end{aligned} \tag{24}$$

Though pressure histories along particular trajectories of flow through a given turbopump could easily be incorporated, there are indications that the solution in terms of the bubble size history is not especially sensitive to the precise *form* of the pressure distribution; of greater importance is the relative magnitude of $(-C_{PM})$ and σ. It is generally recognized that in most cavitating flows the values of these two parameters do not differ greatly.

Since typical cavitation numbers are quite small and C_{PM} is of comparable magnitude, the fluid velocity does not change greatly from its value, U, at $t = 0$. Hence the nondimensional distance along the trajectory, x, can replace t as far as the mean flow is concerned.

The number density of nuclei in the stream in the size range R_N to $R_N + dR_N$ is denoted by $N^*(R_N)dR_N$ bubbles per unit liquid volume where $N^*(R_N)$ is the bubble number density distribution function. It will be assumed that no bubbles are created or destroyed. Then the total bubble volume per unit cross-sectional area of the stream in a length Ldx of the trajectory is

$$\int_{r_N} \frac{4\pi}{3} N(r_N)\{r_0(x)\}^3 L dx dr_N \tag{25}$$

where $N(r_N) = N^* \times L^4$ is the nondimensional bubble number density distribution function.

It will become clear in the analysis to follow that the bubble number density is of considerable importance in assessing the compliance of this form of cavitation. Unfortunately there appears to be little or no data available on the form of this distribution, and none specific to the inflow of cryogenic turbopumps. For want of anything more appropriate, some measurements of bubble numbers in water tunnels by Schiebe [17] and Ripken and Killen [18] have been reduced to the appropriate distribution function form and are presented in Fig. 4. Tentative conclusions based on the *form* of these curves are included in later sections; it is possible however that the numbers of nuclei present in a typical turbopump operation are somewhat greater than in the relatively deaerated water of a water tunnel.

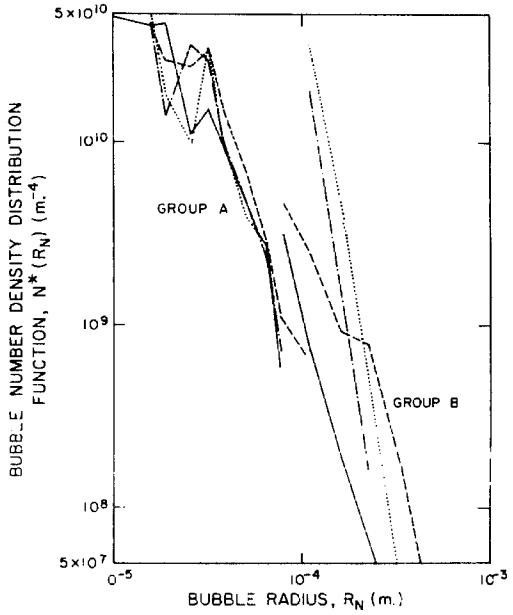

Fig. 4 Some bubble number density distribution functions derived from the experimental measurements of Schiebe[17] (Group A) and Ripken and Killen [18] (Group B)

The above mean flow state will now be perturbed and the change in total bubble volume calculated prior to assessment of the compliance, C_B. A nondimensional compliance is defined by K_B where

$$K_B = C_B \cdot \frac{U^2}{2LA_i}. \tag{26}$$

This is very similar to the form used by Brennen and Acosta [6] for blade compliance; U may be assessed as the relative fluid velocity at inducer inlet, A_i the inlet area, and L as some characteristic length of fluid trajectory through the inducer.

Quasistatic or low frequency results are most easily obtained and are presented prior to the more complete dynamic approach.

6 Quasistatic Analysis of Compliance

In the quasistatic approach to perturbations of the mean flow characterized by $C_{P0}(x)$ and $r_0(x)$ are assumed to take place at such a low frequency, Ω, that the perturbed states are themselves solutions of the mean flow equations. The perturbation is assumed to consist of a small, uniform static pressure change, C_{P1}, so that as shown in Fig. 3

$$C_P^*(x) = C_{P0}(x) + C_{P1}. \tag{27}$$

The inlet flow also experiences this change; hence the corresponding nucleus will assume a slightly different size, r_N^*. However the quantity of gas in this modified nucleus should be the same as in the original; then it follows from equation (7), the upstream conditions and the perfect gas law that

$$\left(\frac{r_N^*}{r_N}\right)^3 = \frac{\sigma + r/\mathrm{We}\, r_N}{\sigma + C_{P1} + 4/\mathrm{We}\, r_N^*}. \tag{28}$$

When the perturbation is small the linearized solution of this equation for r_N^* is

$$\frac{r_N^*}{r_N} \cong 1 - \frac{C_{P1}}{3\sigma + 8/\mathrm{We}\, r_N}. \tag{29}$$

It follows that the bubble motion in the perturbed state is given by the solution of (7) (with $\theta_B = 0$) with r_N replaced by r_N^*, σ replaced by $(\sigma + C_{P1})$ and $C_P(t)$ remaining as $C_{P0}(t)$.

The total bubble volume in an incremental Eulerian liquid volume is given by (25) with $r(x)$ replaced by $r^*(x)$. Thus the change in volume per unit pressure change is easily computed and from the relations (25) and (26) the dimensionless compliance, K_B, is given by

$$K_L(x) = -\frac{4\pi}{3C_{P1}}\left[(r^*(x))^3 - (r_0(x))^3\right] \tag{30}$$

$$K_C = \int K_L(x)dx \tag{31}$$

$$K_B = \int K_C(r_N) \times N(r_N)dr_N. \tag{32}$$

Most of the results will be presented in the form of "unit compliance" or compliance per unit bubble number density, K_C; K_L is termed the local unit compliance.

Some compromise must be made concerning the limits of integration in (31). The nuclei in the stream prior to $x = 0$, $t = 0$ have some compliance as do the remnant bubbles in the flow downstream of the reduced pressure region. However since the local compliance in these regions is small compared with that in the low pressure region and since our interest is the compliance contributed primarily by a turbopump, the integration for K_C is initiated at $x = 0$, $t = 0$ and continued to one of the bubble collapse minimums.

Computed values of total unit compliance up to the first and second bubble collapses are presented in Fig. 5 for various nuclei sizes, r_N, and cavitation numbers, σ. The predominant contribution during the integration comes from the region of bubble maxima; the additional contributions from further bubble rebounds are rapidly attenuated.

The logarithmic plots of K_C with either r_N or σ are close to linear; indeed they roughly follow the empirical relation

$$K_C \cong 10^3 \times r_N^2 \times \sigma^{-\frac{1}{2}}. \tag{33}$$

In order to obtain a total compliance, K_B, which can be compared with experimental observations, a bubble number density distribution function is required; the typical distributions in Fig. 4 suggest a rough empirical relation of the form

$$N(r_N) \approx 10^{-7}(r_N)^{-4} \text{ for } R_N \gtrsim 3 \times 10^{-5}m \tag{34}$$

where the bubbles smaller than $3 \times 10^{-5}m$ are neglected. Taking a typical value for L in turbopumps of 0.3m (so that the distribution is for $r_N \gtrsim 10^{-4}$) the resulting total compliance from (32), (33), and (34) is

$$K_B \cong \sigma^{-\frac{1}{2}}. \tag{35}$$

In actual fact, of course, L will also be dependent on flow quantities such as angle of attack, blade angle, and cavitation number. Nevertheless when the above result is compared in Fig. 6 with the nondimensional experimental values of compliance for the fuel (−F) and oxidizer (−0) pumps of the J2, F1, and H1 rocket engines quoted by Brennen and Acosta [6] the result is quite satisfying considering the inadequacies in the experimental measurements (see Brennen and Acosta), the approximate nature of the present calculation and the lack of data on bubble number densities.

In the next section a more complete dynamic analysis examines the frequency dependence of the bubble compliance.

7 Linearized Dynamic Analysis

Above a certain but as yet undetermined reduced frequency, $\omega = \Omega L/U$ dynamic effects will become important and the individual bubble as it moves along its trajectory will experience a pressure history of the form

$$C_P(x) = C_{P0}(x) + C_{P1}e^{i\omega t} \tag{36}$$

where ω is the dimensionless frequency $\Omega L/U$. Assuming that the pressure fluctuation amplitude, C_{P1}, a real constant, is suf-

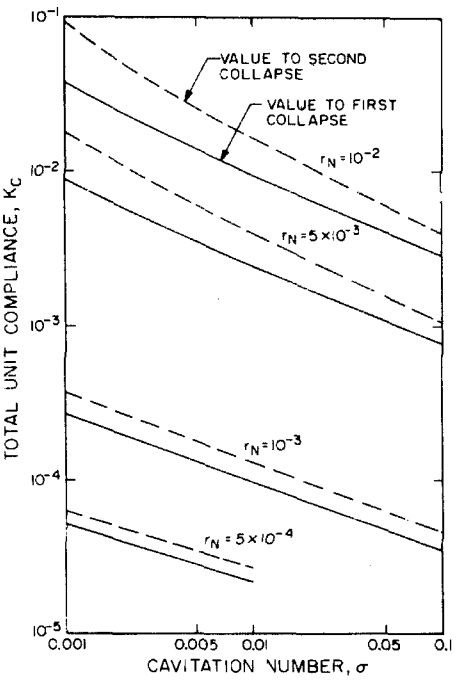

Fig. 5 Quasistatic values of total unit compliance. Solid lines: values to first collapse, dashed lines: values to second collapse.

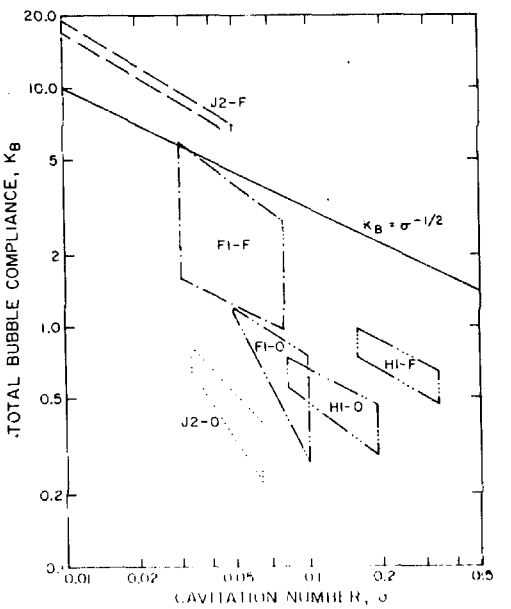

Fig. 6 Comparison of $K_B = \sigma^{-1/2}$ with the experimentally derived total compliances of the fuel (-F) and oxidizer (-O) turbopumps of the J2, H1 and F1 Saturn booster engines

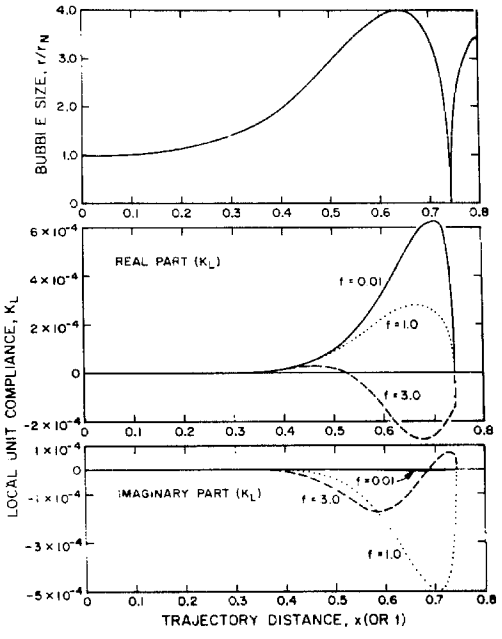

Fig. 7 Values of local unit compliance up to the first bubble collapse for $r_N = 10^{-3}$, $\sigma = 0.01$ and reduced frequencies ($f = \omega/2\pi$) as indicated

ficiently small for a linearized approximation to be valid, then the resulting bubble motion will be of the form

$$r(x) = r_0(x) + r_1(x)e^{i\omega t} \tag{37}$$

where $r_1(x)$ is the amplitude of the radial fluctuations of bubbles at a particular Eulerian position along the trajectory. However, the fluctuations in radius and pressure seen by an individual bubble will be given by (36) and (37) with x replaced by t. Then substituting into (7) (with $\theta_B = 0$), subtracting out the mean motion and neglecting quadratic terms one arrives at the following relation between r_1 and C_{P1}

$$\frac{d^2r_1}{dx^2} + \frac{dr_1}{dx}\left\{2j\omega + \frac{3\dot{r}_0}{r_0} + \frac{4}{\mathrm{Re}\, r_0^2}\right\} + r_1\left\{\frac{\ddot{r}_0}{r_0} - \omega^2 + \frac{3r_N^2(\sigma r_N + 4/\mathrm{We})}{2r_0^5} - \frac{2}{\mathrm{We}\, r_0^3} + 3j\omega\frac{\dot{r}_0}{r_0} + \frac{4}{\mathrm{Re}\, r_0^2}\left\{j\omega - \frac{\dot{r}_0}{r_0}\right\}\right\} = -\frac{C_{P1}}{2r_0} \tag{38}$$

where the dots refer to differentiation of the mean motion $r_0(x)$ with respect to x. This is a linear, second order differential equation whose coefficients are known functions of x once the mean motion has been determined. Solutions for (r_1/C_{P1}) were obtained by means of a complex, second order Runge Kutta procedure. When the compliance given by the expression (30) is similarly linearized it transpires that the local unit compliance K_L is proportional to r_1/C_{P1}:

$$K_L = -4\pi r_0^2\left(\frac{r_1}{C_{P1}}\right). \tag{39}$$

This is easily integrated to obtain the total unit compliance K_C. Both (r_1/C_{P1}) and K_L are in general complex and the results presented later include both the real and imaginary parts.

It is instructive to examine the limiting solution of (38) for high frequencies. Assuming that as ω becomes very large the term $\omega^2 r_1$ on the left-hand side will dominate all other terms it can then be concluded that as $\omega \to \infty$

$$\frac{r_1}{C_{P1}} \to \frac{1}{2r_0\omega^2}; \quad K_L \to \frac{2\pi r_0}{\omega^2}. \tag{40}$$

Thus prior to any detailed results it can be anticipated that as the frequency is increased (i) the real part of the total compliances, K_C and K_B, will shift from an initial positive quasistatic value to negative values which will then tend to zero at large frequencies (ii) the imaginary part will approach zero at both high and low ω, with presumably some maximum (or minimum) at intermediate frequencies.

Calculations were performed only up to the first bubble collapse. Examples of the variation of the real and imaginary parts of the local unit compliance with position x are presented in Figs. 7 and 8 for various reduced frequencies, nuclei sizes and cavitation numbers. These were then integrated to yield total unit compliances, K_C, up to the first minimum and typical values are presented in Figs. 9 and 10 as functions of reduced frequency for several nuclei sizes and cavitation numbers. Also shown in the latter figures are the natural frequencies of the initial nuclei given by

$$\omega_n = \frac{1}{r_N}\left[\frac{3\sigma}{2} + \frac{4}{\mathrm{We}\, r_N} - 2\left(\frac{2}{\mathrm{Re}\, r_N}\right)^2\right]^{\frac{1}{2}}. \tag{41}$$

This can be derived from equation (38) by stipulating the case of a uniform pressure stream ($r_0 = r_N$, $\dot{r}_0 = \ddot{r}_0 = 0$ and $\dot{r}_1 = \ddot{r}_1 = 0$) so that

$$\left(\frac{r_1}{C_{P1}}\right) = \left[2r_N\left(\omega^2 - \frac{4}{\mathrm{We}\, r_N^3} - \frac{3\sigma}{2r_N^2} - \frac{4j\omega}{\mathrm{Re}\, r_N^2}\right)\right]^{-1}. \tag{42}$$

The compliance is again given by equation (39). Incidentally, the expression (42) is similar to the frequency response function of Watts and Hsu [11] when thermal and viscous effects are neglected.

The dotted portions of the curves in Figs. 9 and 10 are less accurate than the rest. Indeed the resonant behavior near the nuclei natural frequencies is not of particular concern here since typical reduced frequencies for the POGO instability appear to be in the range $\omega = 10^{-2}$ to 1 and thus considerably below these bubble resonant frequencies.

One conclusion which can be drawn from Figs. 9 and 10 is that the magnitude of the compliance will decrease from its quasistatic value as the frequency increases. This is at least qualitatively consistent with the trend exhibited by the experimental observations of Fig. 6: it so happens that the reduced

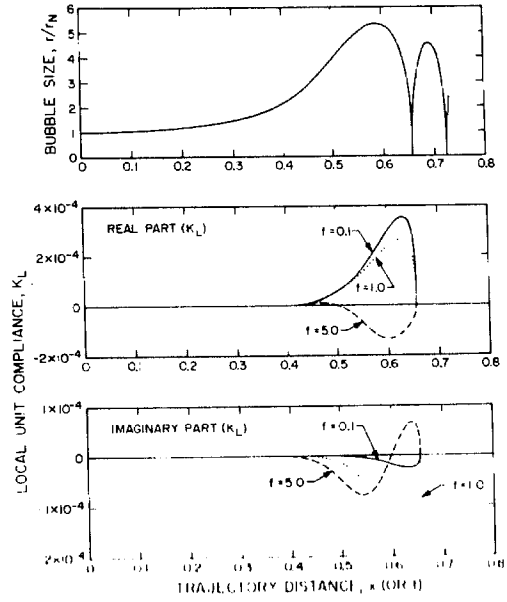

Fig. 8 Values of local unit compliance up to the first bubble collapse for $r_N = 10^{-3}$, $\sigma = 0.1$ and various frequencies ($f = \omega/2\pi$) as indicated

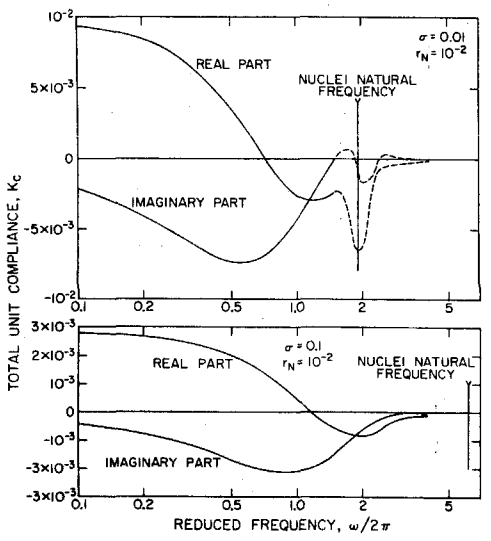

Fig. 9 Frequency dependence of total unit compliance, K_c, for $\sigma = 0.01$ and 0.1 and $r_N = 10^{-2}$.

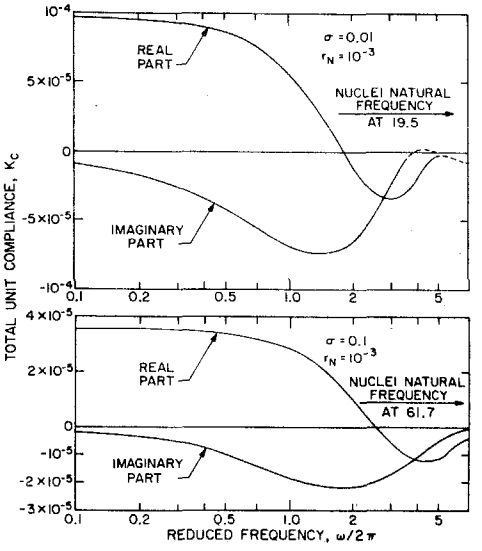

Fig. 10 Frequency dependence of total unit compliance, K_c, for $\sigma = 0.01$ and $\sigma = 0.1$ and for $r_N = 10^{-3}$

frequency for the J2-F results is significantly smaller than for most of the other turbopumps.

8 Thermal Effects on Cavitation Compliance

In order to assess the relative influence of thermal effects on cavitation compliance, the analysis will be confined to flows with uniform mean pressure; thus the objective is to find how the expression (42) is modified. The general perturbations are then

$$C_P(t) = C_{P1}e^{j\omega t},\ r = r_N + r_1e^{j\omega t},\ \theta_B = \theta_{B1}e^{j\omega t} \quad (43)$$

where r_1, θ_{B1} are, in general, complex amplitudes. The appropriate solution to the diffusion equation, (16), assuming a relatively small diffusion layer thickness is

$$\theta = \theta_{B1} \exp\left\{ j\omega t - \left(\frac{j\omega UL}{D}\right)^{\frac{1}{2}} (y - r) \right\}$$

so that

$$\left(\frac{\partial\theta}{\partial y}\right)_{y=r} \cong -\frac{\omega^{\frac{1}{2}}(j+1)}{2}\theta_{B1}e^{j\omega t}.$$

Substitution into the energy equation (15) yields a relation between θ_{B1} and r_1

$$\frac{r_1}{r_N}(\alpha\beta + \sigma + 4/\mathrm{We}\, r_N) = \theta_{B1}\left\{2(1-j)\left[\frac{D^{\frac{1}{2}}c_{PL}T_\infty}{R_N\Omega^{\frac{1}{2}}U^2}\right] + \frac{\beta}{3}\{(\alpha-1)^2 + (\gamma_V - 1)^{-1}\} + \frac{(\sigma + 4/\mathrm{We}\, r_N)}{3(\gamma_G - 1)}\right\}.$$

Finally when this is substituted into the momentum equation (7) the parameter (r_1/C_{P1}) which is proportional to the compliance through the relation (39) is found to be

$$\left(\frac{r_1}{C_{P1}}\right) = -r_N\left[-2r_N^2\omega^2 + \frac{8}{\mathrm{We}\, r_N} + 3\sigma + \frac{4j\omega}{\mathrm{Re}} + \frac{(\sigma + 4/\mathrm{We}\, r_N + \alpha\beta)^2}{\left[2(1-j)\left\{\frac{D^{\frac{1}{2}}c_{PL}T_\infty}{R_N\Omega^{\frac{1}{2}}U^2}\right\} + \frac{\beta}{3}\{(\alpha-1)^2 + (\gamma_V-1)^{-1}\} + \frac{(\sigma + 4/\mathrm{We}\, r_N)}{3(\gamma_G-1)}\right]}\right]^{-1}. \quad (44)$$

This differs from (42) by virtue of the last term which includes thermodynamic properties of the liquid and vapor. It is the magnitude of this term relative to the term 3σ which will be examined in assessing thermal effects. Also it is easily seen that the heat content terms involving γ_V, γ_G contribute little to the denominator of the thermal term. Thus an estimate of the thermal effect is given by comparing the value of the nondimensional function, G, with unity where

$$G = \frac{\left(\sigma U^2 + \frac{2\mathfrak{L}\rho_V}{\rho_L}\right)^2}{3\sigma U^2\left[2(1-j)\left\{\frac{D^{\frac{1}{2}}c_{PL}T_\infty}{R_N\Omega^{\frac{1}{2}}}\right\} + \frac{2P_V}{3\rho_L}(\alpha-1)^2\right]}.$$

Notice that G is a function only of the bubble flow quantities σU^2 and $R_N\Omega^{1/2}$ and the temperature for a particular liquid. In order to display the functional behavior graphically G will be divided as follows

$$G = \frac{F_1}{(1-j)F_2 + F_3} \quad \text{where } F_1 = \frac{\left(\sigma U^2 + \frac{2\mathfrak{L}\rho_V}{\rho_L}\right)^2}{3\sigma U^2} \quad (45)$$

$$F_2 = 2D^{\frac{1}{2}}c_{PL}T_\infty/R_N\Omega^{\frac{1}{2}}$$

$$F_3 = 2P_V(\alpha-1)^2/3\rho_L$$

The component F_1 is a function only of σU^2 and temperature for a particular liquid; its values for three typical σU^2 of 0.1, 10 and 1000 m^2/sec^2 are shown by the solid lines in Fig. 11 for water, liquid hydrogen, and oxygen. The component F_2 on the other hand is a function of $R_N\Omega^{\frac{1}{2}}$ and temperature; its values are indicated by the dotted lines for three values of $R_N\Omega^{\frac{1}{2}}$ of 10^{-2}, 10^{-3}, and 10^{-4} m/sec$^{\frac{1}{2}}$. The component F_3 is a purely thermodynamic function and is shown by the dashed lines.

In order to assess the order of magnitude of G and therefore of the thermal effect, it is first noted that F_3 is unimportant compared with F_2 when $R_N\Omega^{\frac{1}{2}}$ is significantly less than 10^{-2} m/sec$^{\frac{1}{2}}$

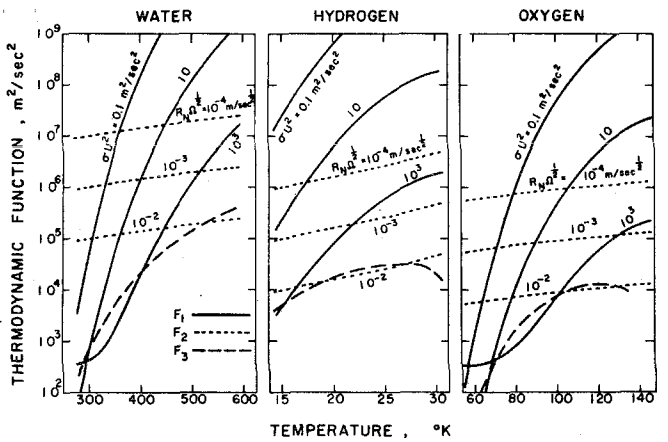

Fig. 11 Thermodynamic function for assessing the thermal effect on bubble compliance:

Solid lines: $F_1 = (\sigma U^2 + 2p_v\mathcal{L}/\rho_L)^2/3\sigma U^2$ **for values of** σU^2 **as shown (in m²/sec²);**

dotted lines: $F_2 = 2D^{1/2}c_{PL}T_\infty/R_N\Omega^{1/2}$ **for values of** $R_N\Omega^{1/2}$ **as shown (in m/sec$^{1/2}$)**

dashed lines: $F_3 = 2P_v(\alpha-1)^2/3\rho_L$.

and this is normally the case. Then it can be concluded from equation (45) that the thermal effect is only significant when $F_1 \geq F_2$. This point is readily determined from Fig. 11 knowing the relevant values of σU^2 and $R_N\Omega^{\frac{1}{2}}$. For example when $\sigma U^2 = 10\text{m}^2/\text{sec}^2$ and $R_N\Omega^{1/2} = 10^{-3}\text{m}/\text{sec}^{1/2}$ there will be a significant thermal effect upon the compliance when the temperature exceeds 400 deg K(127 deg C) in water or 90 deg K in oxygen or at virtually all temperatures in hydrogen.

It can also be concluded from the form of equation (44) that the thermal effect will generally cause a reduction in the value of the quasistatic compliance.

Conclusions

This paper has been concerned, essentially, with the dynamic response of a stream of cavitating bubbles to an applied, oscillating pressure. Both quasistatic and more general dynamic analyses have been made to obtain the cavitation compliance of such flows. Estimated values of the total compliance for the flow through the turbopumps of the rocket engines, J-2, F-1, and H-1 compare favorably with the experimental observation, despite some doubts that surround the validity of the latter and lack of data on the nuclei number density distribution. Auxiliary investigations included in this paper suggest that the following three effects may all contribute to a reduction in the theoretical value of the compliance: (i) thermal restrictions on the mean flow bubble growth during transit through the low pressure region (ii) a large reduced frequency, ω, (greater than about 0.1), and (iii) thermal effects on the oscillatory bubble motion.

Lack of experimental data precludes an assessment of which of these, if any, cause the lower experimental values in Fig. 6. Nevertheless the degree of quantitative correlation and the qualitative behavior of the experimental deviations from the theory strongly suggest that bubble cavitation whether in the backflow of a turbopump or in the mainstream is a major contributor to the cavitation compliance. Systematic analyses such as that presented in this paper should enable estimates of the compliance in a turbopump to be made during the design stage.

Acknowledgments

This work was carried out under NASA Contract NAS8-28046 for whose support the author is most grateful. The encouragement and advice of Professor A. J. Acosta is much appreciated as is that of Professors M. S. Plesset and T. Y. Wu.

References

1 Anon, "Prevention of Coupled Structure-Propulsion Instability (POGO)," NASA SP-8055, Oct. 1970, NASA Space Vehicle design criteria (structures) report, National Technical Information Service, Springfield, Va.

2 Rubin, S., "Longitudinal Instability of Liquid Rockets Due to Propulsion Feedback (POGO)," *Journal of Spacecraft and Rockets*, Vol. 3, No. 8, Aug. 1966, pp. 1188–1195.

3 Ghahremani, F. G., "Turbo-Pump Cavitation Compliance," report TOR-0059 (6531-01)-2, Sept. 1970, The Aerospace Corporation, El Segundo, Calif.

4 Acosta, A. J., "An Experimental Study of Cavitating Inducers," *Proceedings of the Second Symposium on Naval Hydrodynamics*, ONR/ACR-38, 1958, pp. 533–557.

5 Acosta, A. J., and Hollander, A., "Remarks on Cavitation in Turbomachines," Report E-79. 3, Oct. 1959, Engineering Science Department, California Institute of Technology, Pasadena, Calif.

6 Brennen, C., and Acosta, A. J., "Theoretical, Quasistatic Analyses of Cavitation Compliance in Turbopumps," *Journal of Spacecraft and Rockets*, Vol. 10, No. 3, Mar. 1973, pp. 175–180.

7 Brennen, C., and Acosta, A. J., "A Note on Turbopump Blade Cavitation Compliance for the POGO Instability," Polyphase Flow Forum 1972, ASME, Mar. 1972, pp. 23–24.

8 Kim, J. H., "Analysis of Unsteady Cavity in Internal Flows," Polyphase Flow Forum 1972, ASME, March 1972, pp. 25–26.

9 Vaage, R. D., Fidler, L. E., and Zehnle, R. A., "Investigation of Characteristics of Feed System Instabilities," Interim Report MCR-71-278, Sept. 1971, Martin Marietta Corporation, Denver, Colo.

10 Ghahremani, F. G., "Pump Cavitation Compliance," Cavitation Forum 1971, American Society of Mechanical Engineers (ASME) publication, 1971, pp. 1–3.

11 Hsu, Y. Y., and Watts, R. G., "Behavior of Vapor Bubble in a Pulsating Pressure Field," *Proceedings of Fourth International Heat Transfer Conference*, 1970, Vol. 5, Paper B2.4.

12 Plesset, M. S., "Bubble Dynamics," in *Cavitation in Real Liquids*, 1964, editor-R. Davies, Elsevier Publishing Company, Amsterdam.

13 Plesset, M. S., "Physical Effects in Cavitation and Boiling," 1957, Chapter XII, Naval Hydrodynamics, Publication 515, National Academy of Sciences, National Research Council.

14 Plesset, M. S., "Cavitating Flows," Report No. 85-46, Apr. 1969, Division of Engineering and Applied Science, California Institute of Technology, Pasadena, Calif.

15 Stinson, H. P., and Strickland, R. J., "Experimental Findings From Zero-Tank Net Positive Suction Head Operation of the J-2 Hydrogen Pump," NASA TN D-6824, Aug. 1972, George C. Marshall Space Flight Center, Ala.

16 Hord, J., Anderson, L. M., and Hall, W. J., "Cavitation in Liquid Cryogens. I-Venturi," NASA CR-2054, May 1972, NASA Contractor report prepared by National Bureau of Standards, Boulder, Colo.

17 Schiebe, F. R., "The Influence of Gas Nuclei Size Distribution on Transient Cavitation Near Inception," Report No. 107, May 1969, St. Antohony Falls Hydraulic Laboratory, University of Minnesota.

18 Ripken, J. F., and Killen, J. M., "A Study of the Influence of Gas Nuclei on Scale Effects and Acoustic Noise for Incipient Cavitation in a Water Tunnel," Tech. Paper No. 27, Series B, Sept. 1959, St. Anthony Falls Hydraulic Laboratory, University of Minnnesota.